A R C H I V E S O F M E T A L L U R G Y A N D M A T E R I A L S
Volume 54 2009 Issue 1

J. MOLIMARD*, M. DARRIEULAT*

QUANTITATIVE ANALYSIS OF HETEROGENEITIES OF DEFORMATION WITH THE GRID METHOD

ILOŚCIOWA ANALIZA NIEJEDNORODNOŚCI ODKSZTAŁCENIA Z ZASTOSOWANIEM METODY SIATEK

The article deals with the measurement of heterogeneous deformations during the plastic flow of metals. To encode de surface of the test-pieces, transferable carbon grids were used. They proved a reliable technique in the conditions of the experiments (channel-die, step of 100μm), even for highly localized deformations. To calculate the displacement field, the grid method was chosen. Up to now it has been developed for elastic structures. It is extended here to large displacement situations. Results are analysed from a metrological point of view and the resolution is kept at $1/100^{th}$ fringe, the final spatial resolution being at two fringes. The mean deformation is 15% between each loading step. Displacement maps, or better, principle shear strain maps, derived from the previous ones, show the presence of a preferential direction even at low deformation levels. They put forward the decisive role played in the development of heterogeneities by the corners of the test-piece, sensitive in channel-die compression because two of their faces are submitted to friction while the third is free. This first attempt of using the grid method for large displacements will be optimized in the future by automating the iterative procedure and reducing the calculation time.

Keywords: transferable grids; grid method; channel-die; large displacements

Praca dotyczy pomiarów niejednorodnych odkształceń podczas plastycznego płynięcia metali. Na powierzchnię próbek naniesiono siatki węglowe; stwierdzono ich dobrą przyczepność w warunkach prowadzonego eksperymentu (nieswobodne ściskanie w kanaliku – channel die, krok równy 100μm) również dla silnie zlokalizowanych odkształceń. Metoda siatek została wybrana celem wyliczenia pola przemieszczeń. Dotychczas ta metoda używana była tylko w przypadku struktur sprężystych. W pracy rozszerzono zastosowanie metody do przypadku dużych przemieszczeń. Rezultaty są analizowane z metrologicznego punktu widzenia a rozdzielczość metody utrzymuje się na poziomie 0,01 oczka, końcowa przestrzenna rozdzielczość osiąga dwa oczka. Średnie odkształcenie wynosi 15% między każdym krokiem obciążenia. Mapa przemieszczeń, albo inaczej, mapa głównych odkształceń postaciowych, wyznaczona z tej pierwszej, pokazuje obecność uprzywilejowanych kierunków również na poziomie małych odkształceń. Mapy wskazują na decydującą rolę naroży próbki w rozwoju niejednorodności, które są wrażliwe podczas nieswobodnego ściskania (channeldie), ponieważ dwie z trzech ścian próbki są poddane tarciu, a trzecia ściana jest swobodna. To pierwsze osiągnięcie przy zastosowaniu metody siatek do dużych odkształceń zostanie zoptymalizowane w przyszłości dzięki zautomatyzowaniu procedury iteryzacji i zredukowaniu czasu obliczeń.

1. Introduction

The deformation of metals in the plastic range is accompanied by heterogeneities which have been the subject of intense research, from the metallurgical and the mechanical point of view alike [1, 2, 3]. These studies have put in evidence that the causes of these heterogeneities are both 'intrinsic' and 'extrinsic". The former relates to the modes of deformation of the material itself, for example changes in the activity of the dislocations at the origin of micro shear bands [4, 5]. The latter are produced by the boundary conditions imposed on to the test piece by the testing machine [6]. Even mechanical tests, however carefully designed to produce homogeneous fields of deformation, do not escape the effects of friction which triggers heterogeneities of its own.

Getting a quantitative assessment of the field of plastic displacements implies several requirements. The field must be measured on at least one whole face of the test-piece since the edges transmit the efforts imposed on the metal. The order of magnitude of the surface to be covered is the cm^2. Samples being polished to avoid the detrimental effects of scratches, some markers have to be put upon them. To form an image that can be easily

* FRANCE ECOLE NATIONALES SUPÉRIEURE DES MINES DE SAINT-ETIENNE, CENTRE SCIENCES DES MATÉRIAUX ET DES STRUCTURES', UMR CNRS N° 5146, 158, COURS FAURIEL, 42023, SAINT-ETIENNE, CEDEX 2

seen at one glance, 10^4 to 10^6 points are a reasonable choice, which means that the average distance between two of them ranges from 0.1 down to 0.01 mm. In these conditions, information on heterogeneities three or five times larger is yielded. For metals, this is typically the mesoscopic range.

With substrates devoid of natural, regular patterns are a natural choice. With the development of photomechanics, several techniques have been made available to extract the displacement field and its gradient from successive images. Among them is the grid method (GM), used from the beginning of the nineties and described below in this paper. As its name indicates, it implies the deposition of a grid upon the test-piece. Up to now, the GM has been extensively employed in the field of elasticity but never, to the best of the authors' knowledge, in the plastic range. As noted above, the latter is characterized by heterogeneities which produce local deformations far beyond the global deformation imposed by the testing machine. 3D displacements imply specific difficulties of treatment so it was decided for this first attempt to choose a mechanical test in which the initially plane surface of the test-piece remains plane. The channel-die compression was chosen and a grid was deposited upon the face which remains in contact with the wall of the appliance, as described below.

So, Point 2 the paper below presents the technique of deposition of the transferable carbon grids, Point 3 the GM in its classical applications, Point 4 its adaptation to large displacements. Point 5 shows how it could be applied to the first steps of channel-die compression. Point 6 draws a few conclusions on the techniques employed and on the early manifestations of the plastic heterogeneities. Extra considerations on the transferable carbon grids are given in Appendix.

2. Transferable carbon grids

As a result of a transfer of technology from microelectronics, fiducial grids have been used for the first time in 1976 in the field of materials science to put in evidence the displacements at the surface of a metal [7]. Such grids were made of gold and electro litho deposited in a scan microscope. The step of the grid could be any size from 2μm . This process yields excellent results [8]. Nevertheless, because of the aperture of the microscope chamber, the surface covered cannot exceed a few mm^2 at a go. Lining up two sets of grids on the same sample involves considerable difficulties. Thus it was decided to resort to another technology to cover larger surfaces.

Transferable carbon grids (sometimes called also 'pre inked' grids) are made of a polyester film about 0.1 mm thick covered by a photographic emulsion. In a photo plotter a laser beam typically 10 μm wide, positioned with an accuracy of 2 μm , impresses the grid upon the emulsion. There is a dull and a bright face; the former applies on the substrate, the latter bears a criss-cross of carbon bars which form the grids. The contact between the grid and the test-piece is ensured by a glue which polymerizes when heated. It adheres more tightly to the grid than the polyester film so that the latter can be taken off easily, leaving the carbon bars stuck in the glue on the test-piece.

Here are a few details on the procedure followed in the experiments documented below. The substrate was aluminium. The manufacturer of the grids, whose site can be found in [9], provided sheets of grids with steps of 100 μm (30μm are also available). The width of the bars was approximately 50μm . The size of the sheet was of a few dm^2, so that the grids had to be cut off with scissors to overhang by a few millimetres. This was ordinary the size of two samples which were processed at the same time.

The surface of the test-piece was carefully polished and cleaned. A drop of cyanoacrylate glue Loctite 454™ was deposited at its centre and spread out with a spatula. The vendor's specifications can be found in [10]: see in particular its mechanical resistance (15 MPa). The grid was cleaned on its dull face with ethanol, dried with pure air and applied slowly on to the metal to avoid air bubbles. At this stage, it was often necessary to rotate it slightly after the application to ensure the parallelism of the bars with the edges of the test- 5 - piece. Then a small pressure (order of 0.1 MPa) was applied to it and it was kept in an incubator at 26° C during two days. After this, the polyester film was pulled carefully, starting from one edge, until it was completely removed.

The procedure above requires care but proved quite reproducible. The global deformation was measured as $\overline{\varepsilon} = \mathrm{Ln}\left(\frac{h_0}{h}\right)$ where h_0 is the initial height of the test-piece and h the current one. In the present paper, the displacement field is analysed up to $\overline{\varepsilon} = 0.30$ but locally, the deformation can be much larger. Fig. 1 shows a square of grid of 1 mm^2 before (a) and after (b) deformation. With high solicitations, defects may appear at the edges of the testpiece, as detailed in the Appendix.

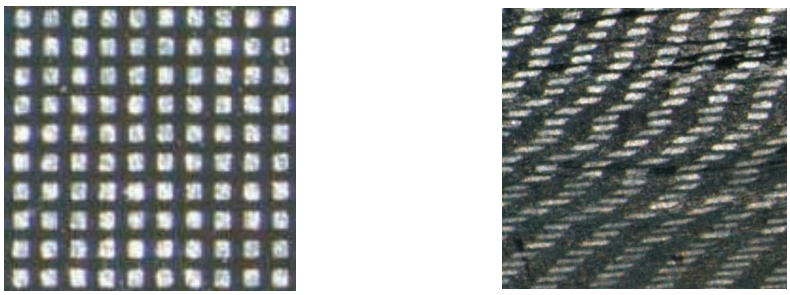

(a) (b)

Fig. 1. Grid (a) before deformation (b) locally deformed at $\overline{\varepsilon} = 0.75$

3. The gird method (GM)

3.1. Choice of an optical full field method

Since the surface is encoded using a periodic pattern, a decoding algorithm is needed to identify displacement and strain fields. Among the various possibilities, two are considered below.

The grid method (GM) is derived from the well-known Moire Geometry technique: the surface is encoded with a periodic pattern. The variations of this pattern are analysed through the extraction of a phase either using global Fast Fourier Transform, or a local approach, for example with wavelet transform [11], temporal phase stepping [12], or spatial phase stepping [13]. Here only the wavelet transform is used, which is an attempt to generalize the spatial phase stepping. Its remarkable signal to noise ratio permits the measurement of very small displacements (typically $1/100^{th}$ fringe, i.e. $5/100^{th}$ pixel) in good conditions. Besides, this method merges the initial and the final frame of reference, and, consequently, it is well adapted to most of elasticity problems [14, 15, 16].

More recently, Digital Image Correlation (DIC) became very popular within the geometric Optical Full Field Methods (OFFM) [17]. This technique deals with random patterns, or with the natural texture of the analysed surface. Thus, it is easier to implement on the one hand. On the other hand, the signal to noise ratio is worse, implying relatively large correlation sub-images (8 to 64 pixels) compared to the wavelets used to analyse periodic patterns (4 to 17 pixels); moreover, a sub-pixel interpolation algorithm is required to reach the same resolution as for the GM. Last, the given result is the mean displacement of each subimage in its initial frame of reference. Then, the natural application field of DIC is large displacement problems (plastic deformation [18], fibrous media [19] ...).

Nevertheless, DIC and phase analysis using wavelet transform are close together and can be sometimes used indifferently [11]. For example, when studying a micro scale structure, if its texture is not rich enough, it is necessary to add a synthetic pattern. For practical reasons, they are usually periodic, for instance concentric circles, or grids. Part of these micro scale analysis deal with ultimate material properties (formability, damage initiation and propagation ...), implying large displacements. Considering this criterion, DIC is a good choice. But, because of the pattern periodicity, the intercorrelation product gives many maxima, and an - 7 - external criterion has to be added, usually point by point, by the user. Actually, this method has been widely used [20, 21].

But, the pattern periodicity, been a default for DIC as described before, can be used using wavelet transform, as it is for the GM. The first results are easy if the displacements remain small. If it is not, the approach has to be adapted in order to deliver displacements in the initial frame of reference. This paper presents in Point 4 below a method to achieve this goal: this will lead to an optimized periodic pattern decoding algorithm for large displacement context. Before, the way it is classically used for small displacements is set out in detail.

3.2. Classical approach for small displacements

The GM combines classically a spatial phase extraction using wavelet transform and a period encoding of the surfaces. The pattern can be applied using transfer technique [22], as in the experiments analyzed below, surface scratching, or photolithography [20]. Depending on the process, the typical grid size is different, varying for macroscopic to microscopic scale (grid step from 1 mm to 2 μm).

If the grid pattern is recorded using an appropriate numerical system, the intensity map on the specimen surface can be written for each point M(r, s) as:

$$I(r,s) = \overline{I}\left(1 + \delta frg\left(\frac{2\pi}{p_r}r + \varphi\right)\right) = \overline{I}(1 + \delta frg(\Phi)), \quad (1)$$

where Φ represent all the differences between the physical fringe pattern and the fringe function frg. Without any stress, this term comes from the set-up defaults (such as a slight camera/grid rotation, or grid specific signature), and consequently remains constant over the test. Under mechanical stress, a point M, originally located at co-ordinates (r, s) is translated at $(r + \delta r, s + \delta s)$. The intensity, expressed in the camera co-ordinates system, becomes:

$$I(r,s) = \overline{I}\left(1 + \delta frg\left(\frac{2\pi}{p_r}(r - \delta r(r - \delta r, s - \delta s)) + \varphi\right)\right). \tag{2}$$

Under small displacements assumption, points (r, s) and $(r - \delta r, s - \delta s)$ are close enough to be merged. Then the phase difference between two different mechanical situations is proportional to the displacement:

$$\Phi_f(r,s) - \Phi_i(r,s) = \frac{2\pi}{p_r}\delta r \quad . \tag{3}$$

In the following, this phase is obtained from the comparison of the intensity levels around a given point. If the intensity variation is supposed to be sinusoidal, the wavelet transform is analogous to the Discrete Windowed Fourier Transform proposed by Y. Surrel [13].

$$\varphi_r = \arctan 2\pi \frac{\sum_{k=1}^{n_x p_x} W_i(k)\sin\left(k\frac{2\pi}{p_r}\right) I\left(r - \frac{n_r p_r}{2} + k\right)}{\sum_{k=1}^{n_x p_x} W_i(k)\cos\left(k\frac{2\pi}{p_r}\right) I\left(r - \frac{n_r p_r}{2} + k\right)}, \tag{4}$$

where:

- n_r : number of periods used,
- p_r : analysis step, close to the real pattern step,
- W_i : local weight applied to each point, describing here a bi-triangular window,
- I : intensity level for each map,

The classical GM has been applied to various mechanical problems, among the most recent: study of damage propagation around a hole [16], Z-pinning on a T-shape specimen [15], or damage structure repairing with optimal composite patches [14]. For all these works, a small displacement assumption is valid; moreover, one can remark that, the grid been ideal, the displacement is measured in the final frame of reference.

4. Adaptation of the GM to large displacements

4.1. Large displacement analysis

In the classical approach described before the phase difference is performed at the same pixel position. In the large displacement situation, the pixel position in the deformed map has to be recovered in some way, to compensate for the rigid body motion. Then, the phase difference can be calculated and gives the remaining displacement between undeformed and deformed states. Note that the present work is focused on large displacements, but do not fix the large strain problem. In fact, this latter affects the pattern wavelength. Consequently, it can become a physical limitation if the grid step is lower than 3 pixels. Another limitation is the presence of harmonics of the chosen grid step, thus a strain rate around 50 %.

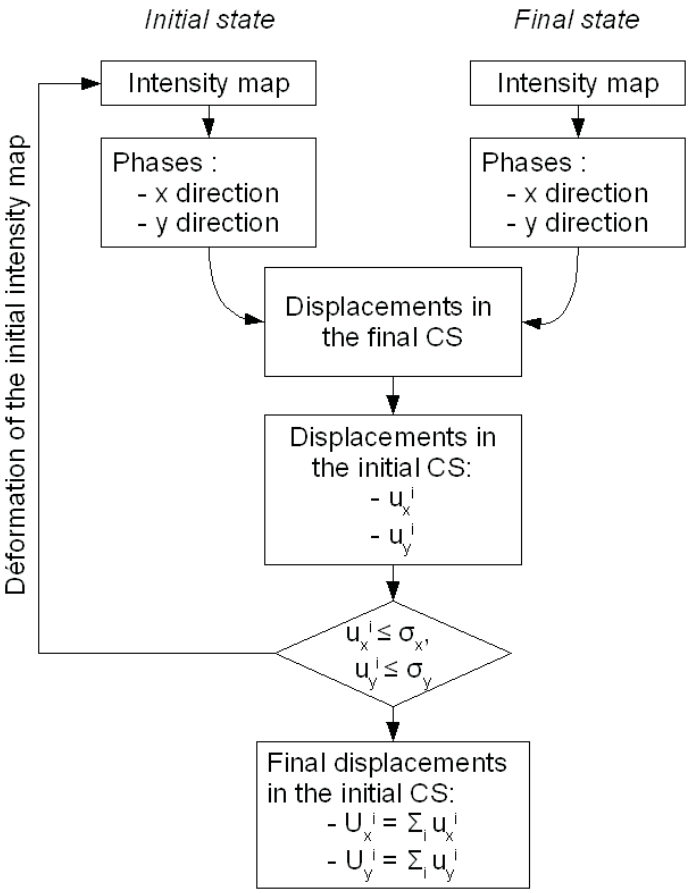

Fig. 2. Extraction algorithm

The strategy adopted here is an iterative procedure, presented on Fig. 2. It is based on the comparison of a numerically deformed map and the mechanically deformed one. At each step, the phase difference maps are calculated, then the relative displacements between the numerically and the experimentally deformed maps. These relative displacements maps are combined with the former displacement maps, and these new displacements are used to deform the initial map for the next step. Then, the right displacement appears to be the sum of each particular displacement map, corresponding to each iteration, in x and y direction. The convergence is achieved when the difference between the numerical

and the experimental maps is close to the optical system resolution.

In this procedure, the difference between the numerically and the mechanically deformed maps is performed using the classical GM. One should pay attention to the coordinate system at each step: the difference is expressed in the final co-ordinate system, and it has to be written in the initial co-ordinate system. Last, the numerical deformation is performed using linear interpolation over a Delaunay triangle. This iterative procedure converges in 3 steps. The first one can be forced to be the mean strain applied to the surface; the second one the low-frequency component of the displacement maps; the last one corresponds to the high-frequency component of the displacements. One should note that the final displacement should be absolute. We use here diamond indents to adjust roughly the two images, and a novel unwrapping procedure, allowing discontinuities (cracks). The calculation time is 5 minutes on a basic laptop (Pentium 1.6 GHz, 500 Mb RAM).

4.2. Error analysis

The present method is an extension of the GM, which have been extensively commented by Surrel [13]. The algorithm used here (WFT) is a self-calibrating algorithm, and isn't sensitive to linear grid step variation. The phase extraction shows that a standard deviation close to $1/100^{th}$ grid step is commonly recorded using a repeatability test. This test is performed at the beginning of each experience. Under small displacements condition, the phase extraction could show a bias related to the presence of harmonics. This error, related to a non-sine pattern signature, can be minimized by mean of a slight image defocusing.
Punctual surface defaults, such as dark spots, scratches could add some perturbations on the phase maps. These defaults being invariant during time, and small displacements condition being achieved, the induced noise is compensated from the reference to the deformed map. But, for displacements larger than the default size, this compensation doesn't occur any more, and a simple repeatability test underestimates the error. Here, because we numerically deform the reference map to obtain the best superimposition on the deformed map, the errors due to pattern defaults are correlated again, and then compensated.

As a matter of fact, the errors on displacement fields, and in particular on the initial image deformation pattern, are not cumulative, and the last error is the only one to be considered. The final error evaluation is given in the final frame of reference; then its evaluation in the initial frame of reference depends on the quality of the interpolation algorithm used. This interpolation being a critical aspect, a numerical evaluation has been performed. A displacement field corresponding to an homogeneous compression test of 0.15, analytically known in the initial frame of reference is defined. The two x- and y- displacement fields and the intensity map are deformed numerically, and expressed in the final frame of reference. The deformed intensity map is deformed again with the reciprocal displacement field, and the two intensity maps (the original one and the twice-deformed one) are compared using the GM. This procedure includes the direct and inverse transformation, as it is in the large displacement framework. In each direction, the mean residual displacement fields are very close to zero (respectively $-1.48.10^{-5}$ and $-4.47.10^{-4}$ pixels in x- and y- direction). The standard deviation characteristic of interpolation errors is very small also, respectively 0.045 and 0.034 pixels. This value is close to the resolution given by the repeatability test for a small displacement case; consequently, it is considered small enough to validate the procedure.

Last, the z-displacement is crucial, as it is already in the case of GM or DIC. It has been shown that an out-of-plane displacement implies a surface dilatation, except if an afocal lens system is used. Here, the images are taken under microscope, out of the mechanical testing machine. All z-displacement variation is related to the focussing, hence the depth of field and the numerical aperture have to be as small as possible to avoid any out-of-plane variation. Last, the studied specimen could induce local variations, depending on the crystallographic situation.

Again, as it already exists in the case of any kind of OFFM, the displacement has to be expressed under physical units, which means the use of a transfer function representing the behaviour of the imaging system. Here, this system is supposed to be perfect, and consequently the pixel size is supposed to be constant over the studied area.

5. Channel-die compression experiments

5.1. Experimental conditions

For reasons given in Point 1, channel-die compression was chosen as a deformation path. Fig. 3 gives the principle of this mechanical test. A die exerts a vertical compression and the metal is forced into a groove between two vertical walls: it flows in the horizontal direction. To avoid friction, the samples are wrapped in a polytetrafluoroethylene film (TEFLON^{TM} was used) about 0.075 mm thick which reduces the friction [23]: indeed, no shear of the grid between the substrate and the TEFLON^{TM} layer seems to take place. The glue is

much more shear resistant than the wrapping, so that the latter absorbs all the friction at the contact with the wall of the channel-die.

Poly and single crystals of Al 1%w Mg were compressed at room temperature. In anisotropic materials like single crystals, the precise geometry of the heterogeneities of the flow depends on the crystallographic orientation and a thorough study of this dependence is in progress. Nevertheless, in all cases, the shapes of the heterogeneities are similar and so are the levels of local deformation. In this paper results from the compression of Goss {110}<001> single crystals are presented.

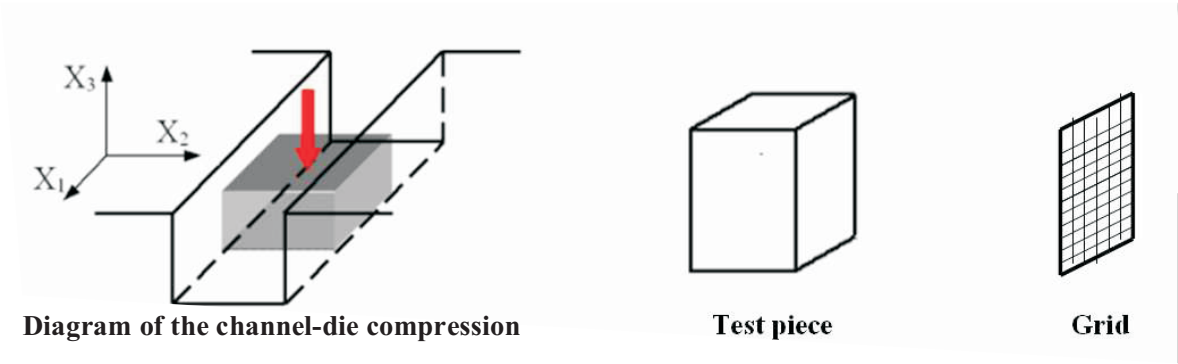

Fig. 3. Channel-die

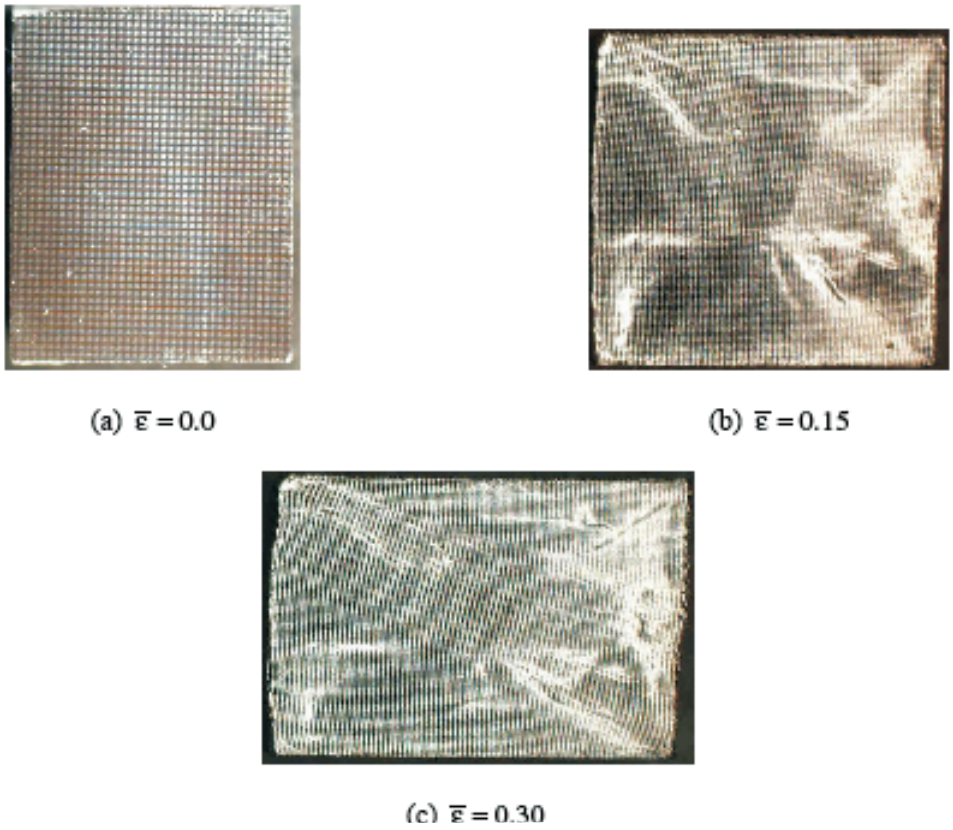

Fig. 4. Test-piece covered with its grid at various stages of its deformation

Initially, the specimen was 10.44 mm high, 8.21 mm long and 7 mm thick. This size avoids buckling and keeps friction low at the same time [24]. The test-piece, whose width is constant, was deformed by steps of E = ln(ho/h) = 0.15. At each step, the specimen was removed from the channel die, the PTFE protection is

changed, and photographs are taken under a binocular lens. Fig. 4 shows the grid at successive steps up to $\bar{\varepsilon}$ = 0.30. A global approach was investigated with a total field view of 11 × 10 mm^2 (773×695 pixels^2). Four diamond micro-indents are stamped at each corner of the grid, to facilitate the centring of the studied area from one load step to the other.

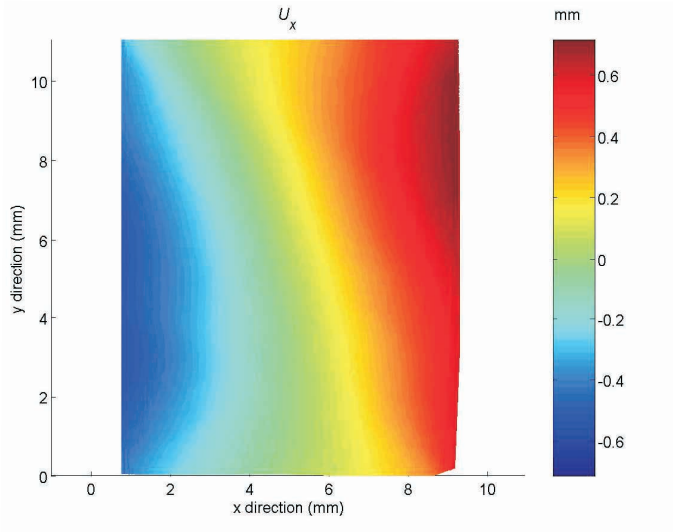

(a) x-displacements – 15% applied strain

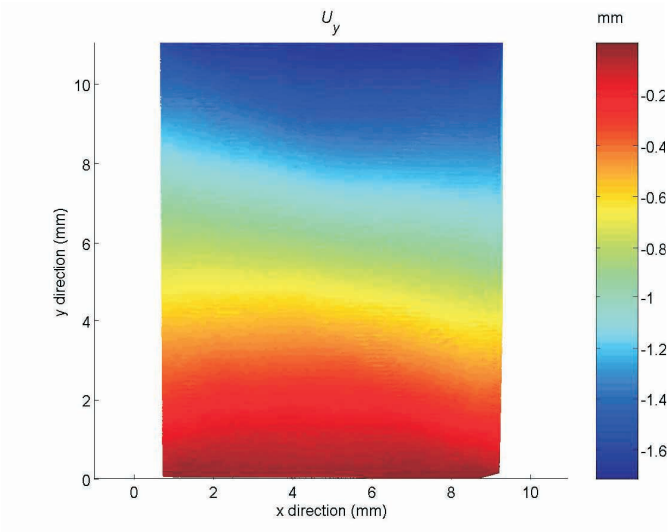

(b) y-displacements – 15% applied strain

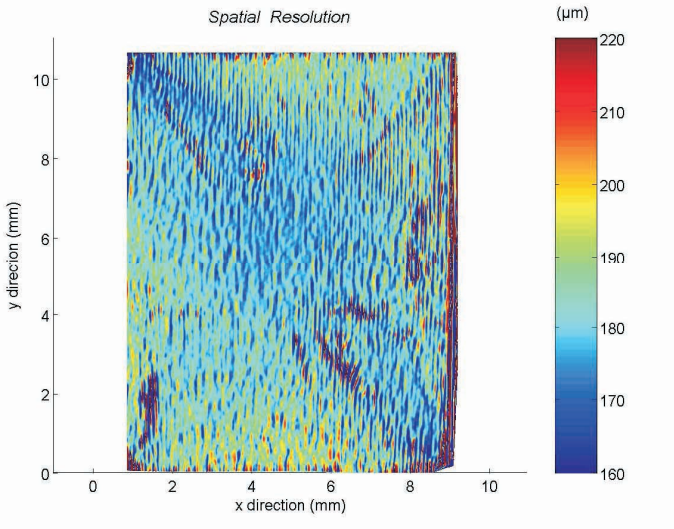

(c) Spatial resolution – 15% applied strain

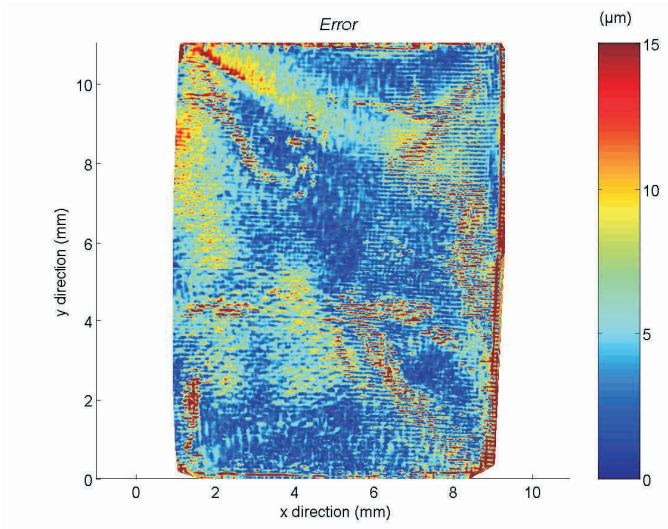

(d) Residual displacements – 15% applied strain

Fig. 5. Analysis of the first step of deformation ($\bar{\varepsilon}$ = 0.15)

Fig. 5 (a) and (b) presents the first displacement ($\bar{\varepsilon}$ = 0.15) obtained using the previously described procedure. The wavelets used are a 9-pixel or a 6-pixel sinus repeated twice, and convoluted by a triangular function, respectively according to the x-direction and the ydirection. No filtering is used at this stage and resolutions are at their best values: 1.28 µm and 0.86 µm in each direction. In the same way, spatial resolutions are minima: 243 and 157 ěm in the final frame of reference. Evaluating the spatial resolution in the initial frame of reference could become a tedious task, because it implies using the inverse transform to spatial resolution fields in the final frame of reference. So far, the spatial resolution characterizes intrinsically a measurement rather than a measurement apparatus or a methodology.

Fig. 5 (c) shows the evolution of the mean spatial resolution at each location in the initial frame of reference. The way to average the spatial resolution according

to x- and direction is a second order norm. It means that the averaged spatial resolution is the diameter of a circle of the same area as the one effectively implied in the definition of each measurement. In the present case, the values remain relatively homogeneous.

The mean spatial resolution is 195 μm, with an anisotropic shape, larger in the xdirection (208 μm, i.e. 15 pixels, in the x-direction, 181 μm, i.e. 13 pixels in the ydirection). The final displacement error is easily evaluated using the difference map between the numerically and the mechanically deformed maps. Figure 5 (d) presents the length of the residual displacement vectors for each measuring point. The mean value, corresponding to a residual rigid body motion, is 0.40 μm, i.e. $3/100^{th}$ pixels. The standard deviation is 0.28 μm. Consequently, when conducted till convergence, this procedure gives results of the same quality as the classical Grid Method.

5.2. Gradient calculation and strain analysis

The gradient calculation is performed using the same procedure as in the case of small displacements case. Previous works from the laboratory have outlined basic rules for the optimization of smoothing length vs. derivation length ratio considering resolution and spatial resolution [25]. The derivation kernel has to be 1.4 times larger than the smoothing kernel. Here, these parameters are tuned in such a way that the spatial resolution on the displacement gradient is 32 pixels (457 μm). The resolution on the gradient is in this case 0.8 %. Even if this value could be found high, it has to be compared to the mean strain (15 %). Last, the Green-Lagrange strain tensor under plain strain conditions is expressed:

$$\begin{aligned} \varepsilon_{xx} &= \left(\frac{\partial U_x}{\partial x}\right)^2 + \frac{1}{2}\left\{\left(\frac{\partial U_y}{\partial x}\right)^2\right\} \\ \varepsilon_{yy} &= \frac{\partial U_y}{\partial y} + \frac{1}{2}\left\{\left(\frac{\partial U_x}{\partial y}\right)^2 + \left(\frac{\partial U_y}{\partial y}\right)^2\right\} \\ \varepsilon_{xy} &= \frac{1}{2}\left\{\frac{\partial U_y}{\partial x} + \frac{\partial U_x}{\partial y}\right\} + \frac{1}{2}\left\{\left(\frac{\partial U_x}{\partial x} \times \frac{\partial U_x}{\partial y}\right) + \left(\frac{\partial U_y}{\partial U_y}\partial x \times \frac{\partial U_y}{\partial y}\right)\right\} \end{aligned} \quad (5)$$

As plain from the very aspect of the grids, ε_{xx} and ε_{yy} do not differ much from the values of the global deformation imposed to the test-piece, that is, the value they should have if the deformation were homogeneous. The horizontal bars of the grids, too, are seldom tilted. On the contrary, there is a considerable slant of the initially vertical bars, hence the interest of calculating the shear strain. Consequently, Fig. 6 reports the principal shear ε_{12} recorded by the OFFM. Each of Fig. 6 (a) and (b) corresponds to the shear variation between step n and step $n + 1$. For all these data, the mean engineering strain is 15%, but it is easy to see that the shear strain distribution is very different. A last step, from 30% to 45% has been recorded without major damage on the grid, but is not presented here for clarity.

First, the very well known cross of the blacksmith is easy to observe on Fig. 6 (a). A certain asymmetry is already present, even at this very early stage of the deformation process. Bands of heavier shear can be observed at the corners. They do not go from one corner to the other, as a simple mechanical explanation could indicate in a case of tools misalignment. The shear band angle, about 35°, is representative of the intrinsic phenomena occurring in the material, and indicates a main weakness direction. The band width should be mentioned at this stage: the phenomenon is poorly localized, as mentioned already by Cordero [26]. On Fig. 6 (b), from 15% to 30% strain, the shear band is much more localised and clearly asymmetric. In this case, the main orientation is no more 35°, but 45°, as a mechanical analysis would predict, and the band spreads around the diagonal of the sample.

It can be seen in this example that the plastic heterogeneities have both an intrinsic and extrinsic character. They take their origin from the friction at the corners of the test-piece but their initial direction, about 35°, cannot be attributed to boundary conditions, but rather to material constitutive instabilities. No explanation is offered of the dissymmetry in the bars of the cross, since the material has been prepared with great care and the Goss single crystals have the same symmetries as the channel-die. For $\overline{\varepsilon} = 0.30$, nevertheless, the influence - 18 - exerted by the tools on the test-piece becomes predominant, and it increases when compression is carried on, as visible on the photographs presented in Appendix.

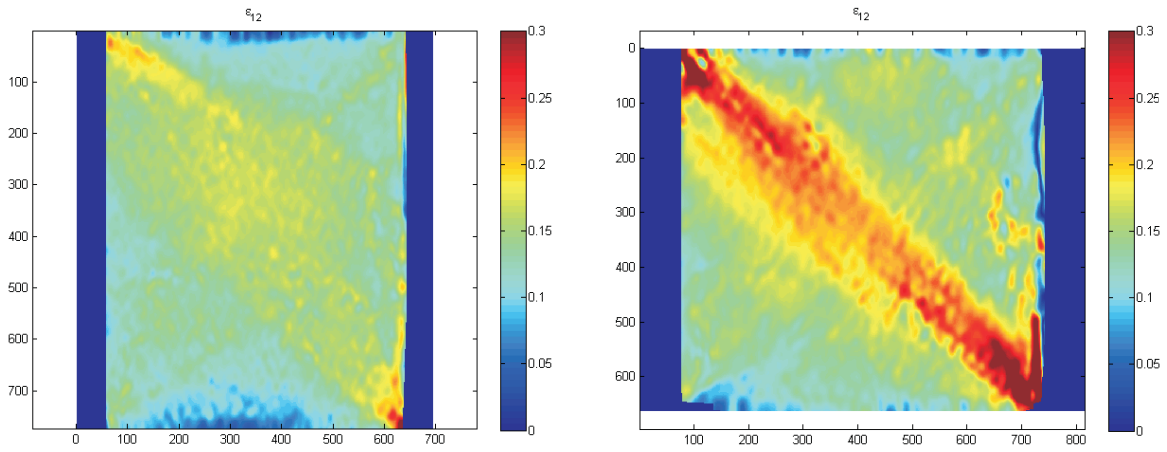

(a). Shear strain – 0 to 15% applied strain

(b). Shear strain – 15 to 30% applied strain

Fig. 6. Analysis of the second step of deformation ($\overline{\varepsilon} = 0.30$)

6. Conclusions

Two complementary techniques have been presented to analyse the field of deformation in the plastic range. The first concerns the deposition of transferable carbon grids which prove satisfactory at large deformation and resist the friction against the wall of a channel-die, provided of course that lubrication is carefully carried out.

The second concerns the grid method, one of several optical full field methods. A theoretical comparison between Digital Image Correlation and the GM has lead to the proposal of an extension of the latter to large displacement problems. It presents the main advantage of being a genuine period pattern extraction method, and well adapted to most small scale applications. The measurement quality has been discussed, and its main characteristics are very close to the classical Grid method (Resolution close to $3/100^{th}$ pixels, Spatial Resolution 14 pixels). This approach could become an alternative to DIC, but the procedure has to be automated and speeded up to be comfortable enough for the users.

From the point of view of metal behaviour, this first attempt has shown that at the mesoscopic range, the heterogeneities of deformation are precocious and have a mixed intrinsic and extrinsic character. They take the form of bands initiating at the corners of the test-piece and crossing it. This phenomenon is not visible with the naked eye, as plain when comparing Fig. 4 (c) and Fig. 6 (b). Further work should tell how they involve into the heterogeneities which have been documented at higher stages of the compression, in particular deformation, transition and shear bands.

Appendix 1: Grid behaviour under heavy deformation

Fig. 2 shows that up to $\overline{\varepsilon} = 0.30$, the grids are most satisfactory and that their imperfections are less important than the reflections of the light which weaken the signal at some places. Nevertheless, carrying on the channel-die compression emphasizes the risks of damage along the vertical edges. Fig. 7 gives an example of it. More than one hundred of tests have been done on poly and single crystals alike, up to deformations of $\overline{\varepsilon} = 1.20$. Hence an assessment of the capabilities of the technique of the transferable carbon grids is offered in the present Appendix.

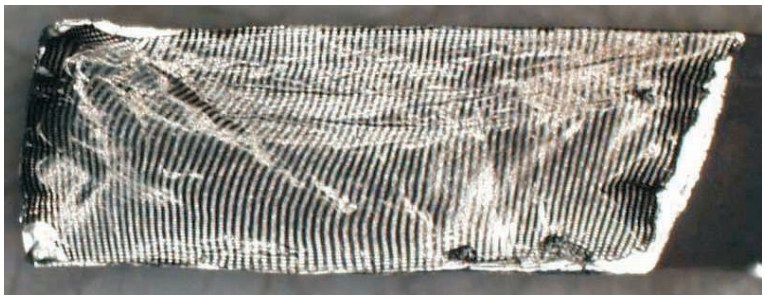

Fig. 7. Tearing at the corners of a sample ($\overline{\varepsilon} = 0.75$)

Far from the edges, the resistance of the grids to the deformation is very good. It may happen that some accidental scratch (for example of the size of a half millimetre) is made to the sample. The resulting crack in the grid does not propagate and its sides follow the deformation of the test-piece. With heavy compression, the distortion may be such that initially vertical bars become wavy and they rotate locally of more than 90°, as shown on Fig. 8. In spite of this, no tearing of the grids was noticed. On the horizontal edges too, at the contact with the die or the bottom of the groove, no damage was noted. The inclination of the bars of the grid reveals the growing friction at their contact with the punch and the bottom of the groove, but the grid remains in good condition, as can be seen on Fig. 8. This figure shows the good condition of the grid when the Goss single crystal used in the experiments above has been compressed up to $\overline{\varepsilon}$ = 0.90. Grids are particularly efficient to reveal the sharp transitions which occur between areas of the substrate which deform differently.

Fig. 8. Distortion of vertical bars, Copper single crystal ($\overline{\varepsilon}$ = 0.90)

The most sensitive parts of the grids are the initially vertical edges. They often tilt because of the anisotropy of single crystals or the fact that with polycrystals, the material at the contact of the upper die flows more than at the contact with the groove [24]. Often too, they become jagged because they form the limit with the free surfaces of the sample. Since the metal is forced into a kind of square-shaped tube, with friction on each side, these surfaces are heavily rugged and the grid deposited on the lateral side of the test-piece may peel off, as seen on Fig. 7 above.

The corners of the grid, too, are especially sensitive to damage. In some tests, at these particular points, the free faces collapse under the effect of the friction on two sides of the test-piece and crush on to the die (as in Fig. 8) or on to the bottom on the groove. Of course this may trigger off tearing in the grid.

These shortcomings are linked to the particular design of the channel-die test. Nevertheless, it is remarkable that the contact with the wall of the channel-die does not damage the inner part of the grid, because of the efficiency of the Teflon^{TM} wrapping (estimated friction coefficient: f = 0.02). A broader assessment of the capabilities of the technique would require a systematic review of the main mechanical tests. Some tests have been done in ordinary compression: no tear was noticed at the surface of a sample in spite of the barrelling characteristic of this deformation path.

The main limitations of the transferable carbon grid are thus the step, which is too large for the analysis of microscopic phenomena and the fact that they do not operate at high temperature, hot deformation being a subject of considerable interest nowadays.

REFERENCES

[1] S. Gorczyca, S. Dymek, J. Ryś, M. Maslanka, M. Wróbel, Arch. Metall., Warsaw **31**, 23-32 (1986).
[2] H. Paul, A. Morawiec, E. Bouzy, J. J. Fundenberger, A. Piątkowski, Met. Mat. Trans. A, **35**, 3775-3786 (2004).
[3] P. J. Hurley, F. J. Humphreys, Acta Mater. **51**, 1087-1102 (2003).
[4] A. Korbel, P. Martin, Acta Metall. **34**, 10, 1905-1909 (1986).
[5] M. Wróbel, S. Dymek, M. Blicharski, S. Gorczyca, Arch. Metall., Warsaw **38**, 195- 203 (1993).
[6] A. Needleman, Revue Phys. Appl. **23**, 585-593 (1998).
[7] D. G. Attwood, P. M. Hazzledine, Metallography **9**, 483-500 (1976).
[8] A. Karimi, Mater. Sci. Eng, **63**, 267-276 (1984).
[9] http://www.laser-techno.com
[10] http://www.stopoxygen.com/downloads/fr/COLLE454.pdf
[11] J. Molimard, A. Vautrin, Proceedings of the CMOI/MTOI Conference, Nov. 2005, Marseille, France, edited by P. Smigielski, 89-90, (2005).
[12] B. Zhao, Ph D dissertation, Université Claude. Bernard, Lyon, France (1994).
[13] Y. Surrel, Applied Optics **35**, 1, 51–60 (1996).
[14] J. D. Mathias, X. Balandraud, M. Grédiac, Applied Science and Manufacturing **37**, 177-190 (2006).
[15] J. Molimard, A. Vautrin, J. M. Béraud, P. Henrat, Proceedings of Comptest (Composites testing and model Identification) Porto, 41-42 (2006) edited online at http://paginas.fe.up.pt/comptest2006/proc/files/boabs.pdf– consulted Nov. 27th, 2008.
[16] F. Pierron, B. Green, M. R. Wisnom, Proceedings of Comptest: Composites testing and model identification, Porto, 112-113 (2006) edited online at http://paginas.fe.up.pt/comptest2006/proc/files/boabs.pdf— consulted Nov. 27th, 2008.

[17] M. A. Sutton, C. Mingqi, W. H. Peters, Y. J. Chao, S. R. McNeill, Image and Vision Computing **4**, Issue 3, 143-150 (1986).
[18] D. Garcia, J. J. Orteu, L. Penazzi, J. Mat. Proc. Tech. **125-126**, 9, 736-742 (2002).
[19] S. Bergonnier, F. Hild, S. Roux **40**, 2, 544-556 (2007).
[20] T. Bretheau, J. Crépin, P. Doumalin, M. Bornert, Revue de Métallurgie-Cahiers d'informations techniques **100**, 5, 567-581 (2003).
[21] D. Chapelle, M. Darrieulat, Mat. Sci. Eng. A **347**, 1-2, 32-41 (2003).
[22] J.-L. Piro, M. Grédiac, Experimental Techniques, 23-26, July/August 2004.
[23] C. Chovet, Ch. Desrayaud, F. Montheillet, Int. J. Mech. Sci. **44**, 2, 343-357 (2002).
[24] C. Maurice, D. Piot, H. Klocker, J. H. Driver, Metall. Mater. Trans. A 1039-1047 (2005).
[25] J. Molimard, A. Vautrin, Proceedings of the CMOI/MTOI Conference, Nov. 2005, Marseille, France, edited by P. Smigielski, 2-3, (2005).
[26] F. Labbé, R. R. Cordero, Opt. Laser Eng. **45**, 1, 153-159 (2007).

Received: 20 December 2008.